ELSEVIER

Chemical Engineering Journal 137 (2008) 84–96

Chemical Engineering Journal

www.elsevier.com/locate/cej

Porous three-dimensional scaffolds made of mineralised collagen: Preparation and properties of a biomimetic nanocomposite material for tissue engineering of bone

M. Gelinsky [a,*,1], P.B. Welzel [b], P. Simon [c], A. Bernhardt [a], U. König [a,1]

[a] *The Max Bergmann Center of Biomaterials Dresden, Institute of Materials Science, Technical University Dresden, Budapesterstr. 27, D-01069 Dresden, Germany*

[b] *The Max Bergmann Center of Biomaterials Dresden, Leibniz Institute of Polymer Research Dresden e. V., Dresden, Germany*

[c] *Max Planck Institute of Chemical Physics of Solids, Dresden, Germany*

Received 5 July 2007; received in revised form 13 September 2007; accepted 17 September 2007

Abstract

For healing of bone defects and as matrix for tissues engineering, porous scaffolds are required that can be easily pre-seeded with cells in the lab and invaded by tissue after implantation. We have developed porous 3D scaffolds consisting of mineralised collagen type I—a nanocomposite, which mimics the composition of extracellular matrix of healthy bone tissue. The steps of material processing as well as the physico-chemical, structural and mechanical properties of this biomaterial are described in detail. The technology of differential scanning calorimetry, which provides an excellent possibility to investigate collagen-based materials, was used to characterise the final scaffold and all its intermediates *in situ*. Furthermore, the interconnecting porosity of the scaffolds with pore diameters of about 200 μm has been shown to be highly suitable for homogenous cell seeding, demonstrated with human marrow stromal cells.

Keywords: Biomimetic; Porous; Scaffold; Hydroxyapatite; Calcium phosphate; Collagen; Nanocomposite; Calorimetry

1. Introduction

Up to now autologous bone graft is still seen as the "gold standard" for the treatment of critical size bone defects [1]. Due to risks and morbidity of the harvesting procedure and the limited available amount, many attempts have been undertaken to develop synthetic bone replacement materials, which overcome the limitations of autologous bone graft—but are as effective concerning their healing capacity. One promising route is the use of materials, which mimic composition and structure of the extracellular matrix (ECM) of bone tissue, consisting mainly of collagen type I and the mineral phase hydroxyapatite (HAP) [2]. Bone (or better: the ECM of bone) can be interpreted as a highly organised composite material. Several different types of bone like compact (cortical), cancellous (spongy, trabecular) and woven bone are known which differ concerning their hierarchical organization, but all types consist at the nanometer scale of a nanocomposite made of collagen type I and HAP [3]. The most organised type is compact bone, in which the mineralised collagen fibres are forming osteons—cylindrical motifs in which the fibrils are aligned parallel to each other in lamellas [4]. Osteons are a consequence of the continuous remodeling of bone tissue; they are generated by osteoblasts, synthesising layer-by-layer new mineralised ECM in the channel-like resorption tunnels, made by the osteoclasts. The structure of the mineralised collagen fibrils on the nanometer level is still not totally clear and subject of intensive research [5]. Known is, mostly from TEM investigations, that (at least for bone of human adults) the HAP crystals are plate-shaped and very small (about 2–4 nm × 25 nm × 50 nm) and mostly located in the gap regions of the collagen fibrils because the typical banding pattern with 67 nm periodicity can be observed in TEM micrographs of unstained bone or mineralised tendon samples [3].

Whereas compact bone has pores only in the micrometer (Haversian channels) or sub-micron level (canaliculi), trabecular bone is a highly porous material in which the orientation and

* Corresponding author. Tel.: +49 351 463 39370; fax: +49 351 463 39401.
E-mail address: michael.gelinsky@tu-dresden.de (M. Gelinsky).

[1] Both these authors contributed equally to this study.

1385-8947/$ – see front matter © 2007 Elsevier B.V. All rights reserved.
doi:10.1016/j.cej.2007.09.029

size of the trabecules are perfectly adapted to the mechanical requirements [6].

An artificial ECM of bone tissue neither has to meet the outstanding mechanical properties of bone, nor to mimic the porosity of (trabecular) bone. Due to the fast resorption of collagen-based materials *in vivo*, such a scaffold first and foremost must be able to act as a suitable matrix for cell seeding and it should be remodelled *in vivo* like natural ECM.

We have developed such biomaterials based on an organised nanocomposite material ("mineralised collagen") in which nanoscopical HAP crystals are deposited on the biopolymer phase during collagen fibril reassembly [7]. First, we synthesised flat, membrane-like "tapes" out of this artificial extracellular bone matrix [8] and studied the growth and osteogenic differentiation of human marrow stromal cells (hMSC) on this material [9]. In addition, we used the tapes to establish an *in vitro* model for bone remodeling by co-cultivation of osteoblasts and osteoclasts, and could show that the latter resorb the mineralised collagen nanocomposite similar to degradation of bone matrix *in vivo* [10].

For the treatment of bone defects, three-dimensional biomaterials are necessary. A fast healing can only occur if the material has pores, suitable for cell and blood capillary ingrowth. Such porous materials can either directly be used as implants or fillers – or, following the tissue engineering approach – as scaffolds for pre-seeding with autologous cells. Using our mineralised collagen nanocomposite and applying controlled freeze drying, followed by chemical cross-linking, we have developed such a porous biomaterial, mimicking structure and composition of the extracellular matrix of healthy bone tissue [11]. In the present study, we describe the preparation protocol, which leads to an interconnecting porous system suitable for homogenous cell seeding *in vitro*. In other publications [12,13], we already have demonstrated that this type of scaffold also enables fast tissue ingrowth *in vivo*. We have characterised all intermediates of the preparation process with the method of differential scanning calorimetry (DSC) and discuss the micro- and nanostructure of the nanocomposite. Finally, some variants of the material are presented.

2. Experimental

2.1. Materials

Prerequisite for formation of the defined mineralised collagen nanocomposite is the use of a collagen type I, soluble in diluted hydrochloric acid. For the scaffold preparation and the subsequent measurements described here, two different collagen sources were used: collagen, isolated from bovine tendon and post-digested with pepsin (kindly provided by Syntacoll, Saal/Donau, Germany—abbr. "tendon") and collagen, isolated from calf skin without pepsin treatment (Collaplex 1.0, GfN, Wald-Michelbach, Germany—abbr. "skin"). If not explicitly mentioned, collagen from bovine tendon was used. HCl, KH_2PO_4 and K_2HPO_4 were purchased from Merck, $CaCl_2$ and tris-hydroxymethyl aminomethane (TRIS) from Roth and *N*-(3-dimethylaminopropyl)-*N*′-ethylcarbodiimide (EDC) hydrochloride from Fluka (all Germany).

2.2. Scaffold preparation

The process, leading to synchronous mineralisation and fibril reassembly of collagen type I, has been described in detail earlier [7]. Capital letters in brackets refer to samples tested in DSC studies described below. To summarise, acid soluble collagen I was dissolved in 10 mM hydrochloric acid (A) and mixed with a 0.1 M calcium chloride solution. The pH was adjusted to 7 by addition of 0.5 M TRIS and 0.5 M Sørensen phosphate buffer (both with a pH of 7.4) and the mixture was warmed up to 37 °C for 12 h. Under these conditions, the collagen fibril reassembly and the formation of nanocrystalline HAP occur simultaneously. The reaction was performed under air whereby the formation of carbonated HAP was not prevented. Under standard conditions the calcium-to-phosphate ratio of the reaction mixture was 1.67 and therefore, similar to that in HAP. For the scaffold preparation normally 1 g collagen is used for the mineralisation and fibril reassembly process in a total volume of 2 l. The product – homogenously mineralised collagen fibrils – was collected by centrifugation as a wax-like, colourless material. To prepare the porous scaffolds described in this study, the mineralised collagen was mixed with mother liquor and stirred up until a just castable suspension was formed (C) which was filled in the cavities of 24 or 48 well polystyrene culture dishes and frozen at −25 °C. The samples were freeze-dried (D) and then cross-linked with a 1% (wt.%) solution of *N*-(3-dimethylaminopropyl)-*N*′-ethylcarbodiimide (EDC) hydrochloride in 80% (vol.%) ethanol for 1 h (E). Afterwards, the scaffolds were rinsed thoroughly in distilled water, 1% glycine solution, once again in water and finally freeze-dried (F). The samples for use in the cell seeding experiment were sterilised using γ-irradiation (dose 30–35 kGy) (G). Cylindrical samples with a diameter of 13 mm and a height of 8 mm were produced for mechanical testing. For DSC measurements, as an additional sample reconstituted, fibrillar, but non-mineralised collagen (isolated from bovine tendon) [7] was prepared (B). Long term storage at room temperature of freeze-dried sample (D) for two years resulted in sample (H) and storage of sample (E) for 4 years is described as (I).

2.3. High performance liquid chromatography (HPLC)

HPLC-based amino acid analysis of mineralised collagen scaffolds has been accomplished as described by Sperling et al. [14]. The carriers were subjected to vapour phase hydrolysis with 6N HCl + 1% Phenol (both from Fluka, Deisenhofen, Germany), at 110 °C for 24 h under reduced pressure. Following hydrolysis the generated primary amines of the amino acids formed derivatives with *ortho*-phthalaldehyde (OPA). Subsequent amino acid analysis of the hydrolysates was performed with a HPLC system (Series 1100, Agilent Technologies, Böblingen, Germany) equipped with fluorescence detector. Hydrolysates and amino acid standards were separated on a reversed phase HPLC column (ZORBAX, Agilent Technologies). Quantification was carried

out using fluorescence detection at 455 nm with excitation at 335 nm comparing the results to a standard amino acid solution as reference.

2.4. FT-IR spectroscopy and thermogravimetry

A pulverised, freeze-dried sample of the porous 3D scaffold, embedded in KBr, was studied by FT-IR spectroscopy with a Perkin-Elmer FTS 2000 (Norwalk, USA). Thermogravimetry (TG) was carried out with a STA 409 instrument (Netzsch Gerätebau GmbH, Selb, Germany). The sample was heated in air at a constant rate of 3 K min^{-1} up to a final temperature of 1300 °C.

2.5. Scanning electron and transmission electron microscopy (SEM and TEM)

SEM was performed with a DSM 982 Gemini electron microscope (Zeiss, Germany, Fig. 10) or a Philips XL 30/ESEM with FEG (field emission gun), operating in SEM mode (Figs. 3 and 15). The samples were mounted on aluminium pins and carbon or gold coated. For SEM of the cell seeded scaffold the specimen was washed twice with warm PBS, fixed for 30 min with 3.7% formaldehyde in PBS, washed with distilled water and dehydrated using a gradation series of ethanol/distilled water solutions. Critical point drying was performed with a CPD 030 apparatus (BAL-TEC AG, Liechtenstein).

For TEM, samples were embedded in epoxide resin. Ultrathin sections of the samples with a thickness of approximately 100 nm were prepared using an ultramicrotome (Reichert, Ultracut, Germany, operated at room temperature) with a diamond knife (DiATOME, USA). The thin sections were deposited on Cu-grids coated with holey carbon foils of Quantifoil with a hole diameter of 3.5 μm. The film size amounted to about 0.2 mm × 0.2 mm. The specimens were investigated by means of a Philips CM200 FEG\ST-Lorentz transmission electron microscope equipped with a field emission gun (FEG), operated at an acceleration voltage of 200 kV. Micrographs were recorded with a 1k × 1k CCD-camera (multi scan, Gatan, USA), and fed to a computer for on-line image processing (Digital Micrograph 3.3.1., Gatan).

2.6. Porosity measurements

The pore size was measured microscopically using thin sections of the scaffolds. For this, the material was embedded in paraffin and thin sections of about 20 μm thickness were prepared with a RM2155 microtome (Leica, Wetzlar, Germany). For better material contrast, staining with hematoxilin and eosin (HE) was done. Porosity was also determined with the method of Hg intrusion porosimetry on an AutoPore IV 9500 machine at low and high pressure (Micromeritics, Germany). Additionally, the quantification of meso- and microporosity according the Brunauer–Emmett–Teller (BET) method (adsorption of nitrogen) was carried out using the device AUTOSORB-1 (Quantachrome, USA) at 77.4 K. Samples ($N = 3$ per scaffold state made of different collagen sources) were prepared 24 h in advance at room temperature by drying under vacuum.

2.7. Synchrotron microcomputed tomography (SRμ-CT)

For SRμ-CT investigation of the porous 3D scaffold one cylindrical sample with a diameter of 6 mm was embedded in polymethylmetacrylate (PMMA). The specimen was evaluated at the BAMline (BESSY II) at the Federal Institute of Materials Research (BAM, Berlin, Germany). For the specimen, 720 X-ray attenuation projections with a local resolution of 3.6 μm were acquired using a X-ray energy of 12 keV. The visualisation and analysis of the reconstructed data was done with a volume rendering software (VGStudio, Volume Graphics, Germany).

2.8. Mechanical measurements

Uniaxial cyclic loading experiments were carried out with the use of an electromechanical Instron 5566 testing machine (Instron Wolpert GmbH, Darmstadt, Germany). The cylindrical samples used had a diameter of 13 mm and a height of 8 mm. They were compressed with a chart speed of 0.3 mm s^{-1} 50 times to half of their original height after swelling in distilled water for 24 h [11]. For non-cyclic measurements, wet samples of the same geometry were compressed up to a load of 50 N with a chart speed of 0.1 mm s^{-1}.

2.9. Differential scanning calorimetry (DSC)

Differential scanning calorimetry was utilised in order to detect collagen denaturation. The measurements were carried out with a Setaram micro-DSC III heat conduction scanning microcalorimeter (Setaram, France). The liquid or solid collagen preparations were placed into the 1-ml measurement ampoule (Hastelloy C). 490 μl of the acidic collagen solution A (corresponding 2.9 mg collagen) and 680–740 μl of the liquid preparations B and C were used. The collagen scaffolds (ca. 28 mg) were immersed in MilliQ water or PBS (730 μl) to keep the collagen fibres in a fully hydrated condition (swollen state) at all time. Absorbed or released heat was recorded relative to the 1-ml reference ampoule filled with an appropriate blank sample (HCl, MilliQ water or PBS). The ampoules were allowed to stabilise at 20 °C/25 °C for 60 min prior to the initiation of the scanning experiment. The temperature program for the collagen starting material was: 20 °C/25 °C → 65 °C → 20 °C/25 °C (and rescanning); for the collagen dispersions 25 °C → 80 °C → 25 °C (and rescanning); for the swollen collagen matrices 25 °C → 110 °C → 25 °C (and rescanning). The heating rate was 1.0 K min^{-1} for all experiments. All measurements were repeated at least once.

We focus the attention principally on the evaluation of the denaturation temperature, which is an intensive parameter, i.e. it does not depend on the actual content of collagen in the sample considered. The denaturation temperature T_d is defined as the temperature at which the local maximum occurs in the excess heat capacity. A higher T_d would reflect an increased stability of the molecules, while a broad shape of the peak and/or the

presence of shoulders would correspond to an increased dispersion in terms of stability of the fibres. For very broad peaks, the temperature range of the transition is given.

2.10. Cell seeding experiments

Human marrow stromal cells (hMSC), isolated from bone marrow aspirate of a healthy donor, were expanded in Dulbecco's Modified Eagles Medium (DMEM) low glucose (Biochrom, Berlin, Germany), containing 10% fetal calf serum (Biochrom), 10 U/ml penicillin and 100 μg/ml streptomycin (Biochrom) at 37 °C in a humidified, 7% CO_2/93% air incubator.

Prior to cell seeding scaffolds from mineralised collagen (10 mm diameter, 7 mm height) were pre-incubated with cell culture medium for 24 h. Thereafter, equilibration medium was removed and samples were placed on a sterile filter paper to remove excess liquid from the pores. Samples were placed in 24-well polystyrene culture dishes and 2×10^5 cells were given within 350 μl of medium to the top of each cylindrical sample. After 1 h of initial adhesion, 1 ml cell culture medium was added to each sample. After cultivation of the cell-seeded scaffolds for 2 and 14 days, the cultures were supplemented with 1.2 mM 3-(4,5-dimethylthiazol-2-yl)-2,5-diphenyltetrazolium bromide (MTT) (Sigma, Taufkirchen, Germany) followed by further incubation at 37 °C for 4 h. The formation of dark blue formazane dye converted from MTT by mitochondrial dehydrogenases of living cells was documented photographically.

3. Results and discussion

Freeze drying of mineralised collagen suspensions, filled in appropriate moulds, leads to porous three-dimensional scaffolds, mimicking the extracellular matrix of bone tissue. Samples can be produced in any size or shape (Fig. 1). Synthesis and properties of this biomaterial will be described below.

Fig. 1. Porous scaffolds, made from mineralised collagen, in different size and shape (the scale shows centimetres).

3.1. Synthesis

The synchronous collagen biomineralisation process, developed in our lab [7], yields a homogenous nanocomposite consisting of reconstituted collagen fibrils and nanoscopical HAP crystals. The growing collagen fibrils act as a template for mineral formation; their presence prevents the precipitation of calcium phosphate particles unconnected to the biopolymer phase. The reaction conditions try to mimic those in physiological systems which include diluted solutions with a typical physiological ionic strength (0.15 mol/l) at pH 5.5–7.5 and $T \leq 40$ °C [15]. The synchronous collagen biomineralisation process is initiated by the precipitation of an amorphous calcium phosphate phase, while the collagen fibril reassembly is starting. During the next few hours, the amorphous mineral phase is slowly transformed to nanocrystalline HAP, which precipitates solely on the collagen template.

After collection of the mineralised collagen fibrils by centrifugation, the porous 3D scaffolds are produced applying a freeze-drying process. For this, a just castable suspension of the nanocomposite is filled in appropriate moulds. Freezing at temperatures between −20 and −25 °C leads to an interconnecting porous system with pore diameters of approximately 200 μm which could be shown to be suitable for homogenous cell seeding (see Section 3.6). Freezing at much lower temperatures led to pores with much smaller diameters, not applicable for cell seeding [11]. Detailed information on the porosity will be given in Section 3.4.

Different methods have been utilised to investigate the exact composition of the mineralised collagen scaffolds. Thermogravimetry of the freeze-dried material (graph not shown) showed that the scaffold contains still about 5% water, which seems to be bound by the collagen phase. At about 200 °C, carbonisation of the organic component starts which is completely burned out at about 500 °C. The collagen content was found to be 28–30%, and the remaining 65–67% consist of the calcium phosphate (HAP) phase. This was also verified by elemental analysis (data not shown) [11]. In addition, composition of the mineralised collagen nanocomposite was investigated by HPLC. With this method, it could be confirmed that the collagen content of the composite is about 30% and the HAP mineral phase makes up 70% (Fig. 2), which is in good agreement with the composition of extracellular matrix of healthy bone tissue [3,16].

Due to the reaction conditions (pH 7, 37 °C, calcium-to-phosphate-ratio = 1.67), HAP should be the only calcium phosphate phase to be formed, which could be verified with several methods [7]. As mentioned earlier, the growing collagen fibrils act as template for the crystallisation of the mineral phase and at the end of the reaction time no unbound crystals can be detected in the reaction mixture (the solution is clear beside the cloudy mineralised collagen precipitation and no powdery precipitate can be found on the bottom of the flask). The FT-IR spectrum (not shown) of the freeze-dried and cross-linked

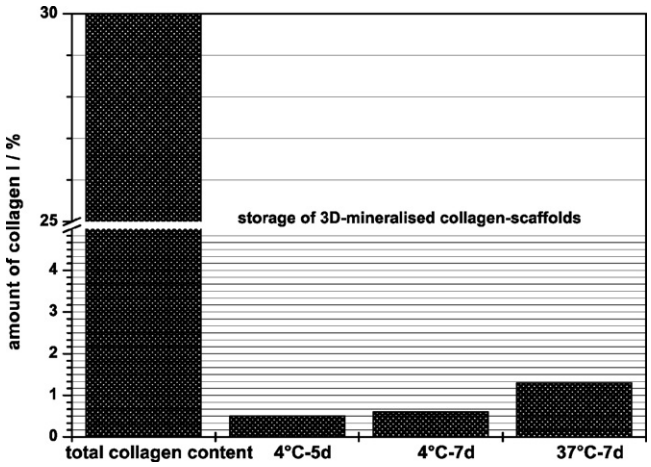

Fig. 2. Determination of the amount of collagen I (source, tendon) of the 3D scaffolds after preparation (total collagen content) and after storage in PBS buffer at different temperatures (4 and 37 °C) after different time ranges (5 and 7 days) by means of the HPLC method.

3D scaffold is rather similar to those of the starting material, mineralised collagen type I [7]. The main absorption bands refer to those of HAP (1028 cm^{-1}) and amide groups of collagen (1673, 1652 and 1558 cm^{-1}). The OH-stretching band of HAP at about 3600 cm^{-1} is concealed by the strong water absorption. No severe band shifts could be detected between the spectra of native collagen type I and that of the mineralised and cross-linked scaffold material (data not shown) which is a strong indication that no denaturation occurs during the whole preparation process. A more detailed discussion of this question based on DSC data is given in Section 3.3. The nature of the calcium phosphate phase was also investigated with HRTEM (see Section 3.4, Fig. 12).

For stabilisation of the open porous structure under wet conditions, chemical cross-linking is necessary. Due to its low toxicity and good solubility, we are using EDC in 80% ethanol for this procedure [17]. The EDC treatment is followed by a washing step with a 1% glycine solution in order to deactivate the excess of activated carboxy groups, which did not interact in terms of cross-linking reaction.

The stability of the mineralised collagen-scaffolds in solution has been studied using HPLC. This evaluation showed that less than 1% of the scaffold material was degraded at 4 °C over a period of 7 days in PBS. The part of dissolved collagen from the mineralised matrix in PBS increased with the storage temperature. We have performed cell culture experiments with the porous scaffolds for up to 8 weeks both under static and perfusion conditions without any problems concerning stability of the material [18]. Nevertheless, in terms of applying the mineralised collagen nanocomposite in the sense of tissue engineering the scaffolds have to degrade after a certain time interval [19]. Animal experiments confirmed a fast degradation *in vivo*; 8 weeks after implantation of the scaffold without pre-seeded cells most of the material was resorbed by osteoclasts when implanted in a bone cavity in rat femur [12].

3.2. Post-mineralisation in simulated body fluid (SBF)

Among the experiments for investigating *in vitro* degradation of the material, the so-called post-mineralisation process has been studied additionally. The incubation of the scaffolds has been carried out in 1.5-fold concentrated SBF [20,21] for different time periods and temperatures. The samples have been washed intensively in distilled water after incubation in SBF in order to remove the excess of salts before they have been used for further investigations. After incubation for 1 month at 4 °C, no morphological changes could be observed, while the storage at 37 °C over 2 days has shown obviously some alteration in the surface morphology. Hereby, the open macroporous structure has been maintained completely, while the meso- and micropores have been modified, as illustrated in Fig. 3. The original and the newly formed mineral phase could be visualised and distinguished by comparison of the SEM images of the scaffold without and after post-mineralisation in SBF. Both dissolution and re-precipitation processes could occur simultaneously in the applied 1.5-fold SBF. However, the elastic properties of the mineralised collagen scaffold were not reduced. Mechanical tests have demonstrated similar results compared to those for the standard material after storage in water for 24 h (see Section 3.5 and Table 2). In contrast, changing the mineral-to-collagen ratio by decreasing or increasing the calcium and phosphate concentrations in the reaction mixture, leading to the mineralised collagen nanocomposite, is impossible. The synchronous collagen fibril reassembly and mineralisation process is running properly only in a small range of concentrations which was already shown previously [7].

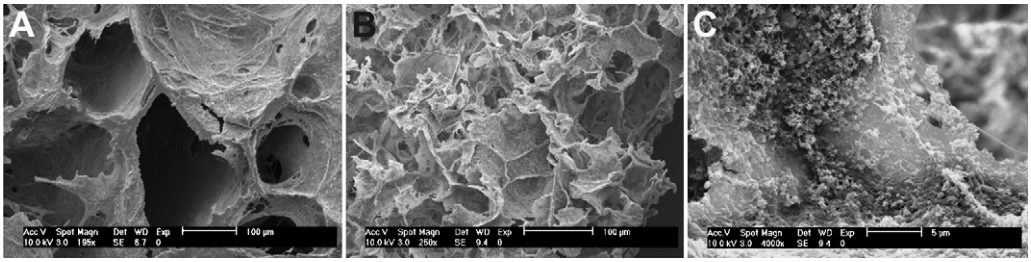

Fig. 3. Observation and comparison of the post-mineralisation after storing the 3D scaffolds of mineralised collagen I at 37 °C in 1.5-fold concentrated SBF solution; here SEM images taken after a storage period of 2 days (B, magnification 250× and C, magnification 4000×) compared with the standard (A, not stored in SBF solution; magnification 195×) are shown.

3.3. Diffential scanning calorimetry (DSC)

DSC experiments can provide information about the temperature T_d of the denaturation process and thus about the thermal stability of the collagen, i.e. the resistance of the protein molecule to unfolding as a result of heat treatment. Thermal denaturation of collagen samples was previously shown to cause the destruction of the triple helix and the unfolding of the separated single peptide strains into random coils [22–24]. The first step of this helix-to-coil-transition involves disruption of water bridges (hydrogen bonds) among the three polypeptide chains of the tropocollagen molecules, while the second step involves the disruption of interhelical hydrogen bonds of α-chains [25].

On the way from the raw material to the scaffolds, several intermediate states were analyzed concerning their thermal stability. The capital letters used for identification are explained in Section 2.2. Furthermore, the effect of sterilisation and storage on thermal denaturation of the collagen triple helix into a random chain was investigated. The data of the scaffolds refer to their swollen states.

Fig. 4 shows an endothermic DSC peak (denaturation) for the acidic tropocollagen dispersion (A) with a maximum at 40.5 °C (shoulder at 35.5 °C). During the subsequent cooling and second heating of the sample, no corresponding peak was detected. The denaturation therefore appears to be complete and irreversible under these experimental conditions. Preparation at room temperature and deeper should preserve the triple helical structure of the starting material. Mu et al. [26] got similar results for the denaturation of collagen solutions in acetic acid and suggested that the shoulder transition and the major transition arise from the defibrillation and denaturation of collagen, respectively. For the mineralised collagen dispersion (C), the denaturation peak is shifted to higher temperatures (T_d = 46.3 °C). This indicates changes in interaction forces due to fibril assembly and mineralisation; aggregation of the collagen (B, caused by a pH and a temperature increase) only increases the denaturation temperature by 2.5 °C (T_d = 43.0 °C). The presence of mineral additionally stabilises the collagen fibres (C). This agrees with several experimental evidences in literature; collagen molecules embedded within the lattice of a fibre are substantially more stable than the same molecules in dilute solution [27–29]. Mineralisation increases the thermal stability of the collagen molecules and the temperature of the transition depends on the degree of mineralisation [30–34]. As the sample (B) shows a high viscosity, sometimes air bubbles are captured in the liquid that are difficult to remove. The heating of the sample above the denaturation temperature results in a release of these bubbles that consequently caused disturbing signals in the baseline after the DSC peak.

The freeze-drying step after mineralisation as a shaping process has no significant influence on the collagen properties (swollen state), as can be deduced from Fig. 4(D) (T_d = 46.1 °C).

A major change in collagen properties results from the cross-linking with EDC (Fig. 5). The cross-linked mineralised collagen in the swollen state (E) is thermally more stable than the non-cross-linked product (D), as can be concluded from the large increase in denaturation temperature (temperature range of denaturation, 60–105 °C). These data indicate stronger association of the collagen fibre structures and support the DSC results of several other authors, who found an increase in denaturation temperature of collagen after cross-linking with various methods [35,36]. Miles et al. [37] stated that cross-linking causes dehydration of the fibres by drawing the collagen molecules closer together and that it is the reduced hydration that causes the increased thermal stability. The width of a DSC peak is an indication of the sharpness of the thermal transition and therefore, the distribution of the collagen population with distinct thermal stability. The broad denaturation peak of (E) may be due to the heterogeneous nature of cross-linking [36] and thus an increased dispersion in terms of thermal stability of the fibres.

The finishing treatment of the scaffolds with glycine (F) does not affect the temperature range of denaturation significantly. Denaturation of the final product (F) takes place far above normal storage temperature and also body temperature, even in the swollen state.

The use of raw materials from different collagen batches results in cross-linked final products with equal thermal sta-

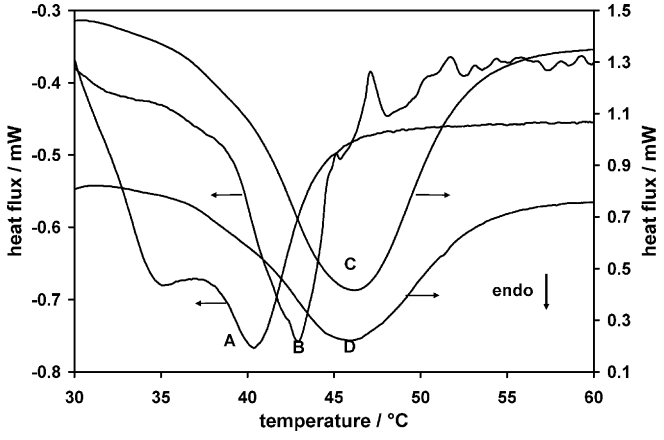

Fig. 4. DSC plots of acidic tropocollagen dispersion (A), fibrillar collagen dispersion (B), mineralised collagen dispersion (C), and freeze-dried collagen scaffold swollen in MilliQ water (D). The horizontal arrows show which scale is related to the respective curve (same in Figs. 5 and 6).

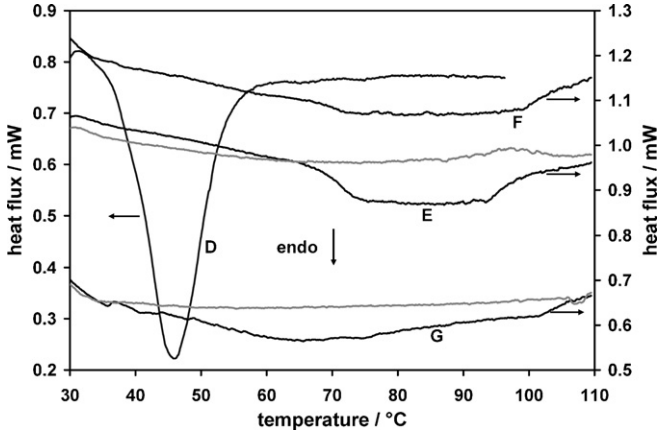

Fig. 5. DSC plots of freeze-dried collagen scaffold swollen in MilliQ water (D), EDC cross-linked collagen scaffold (E), EDC cross-linked collagen scaffold treated with glycine = final product (F), final product γ-sterilised (G); all samples swollen in MilliQ water; grey plots, second heating.

bility. Furthermore, the use of PBS instead of MilliQ water to immerse the final cross-linked collagen scaffold does not have any influence on the DSC curves.

Sterilisation of the final product (F) by γ-irradiation leads to a broadening of the DSC peak (Fig. 5(G)). The denaturation process already starts at lower temperatures (around 37 °C). These findings support the studies of some other authors; Bailey [38] found a decrease in thermal stability of tropocollagen solutions with increasing doses of ionizing radiation (^{60}Co). In addition to the thermally labile molecules, the presence of a portion of undamaged molecules could be demonstrated at doses below 300 Gy. At higher doses intermolecular cross-linking of the collagen molecules occurred. Kubisz et al. [34] reported that γ-irradiation with a high dose (1 MGy) leads to deep structural changes of the bone collagen. Irradiation decreased the hydration level in the bone and its denaturation temperature. The results of the authors showed the domination of the scission of the collagen macromolecules and the degradation process during irradiation. There are also some studies on the effect of UV radiation on the properties of the collagen molecule, in solution or in its aggregated fibrillar form. It has been reported that cross-linking and degradation occur on exposure to UV, the relative proportion depending on the presence of oxygen, pH of solution, type of collagen, wavelength of the UV and irradiation time [39–41].

Cooling of the collagen samples to their initial conditions and rescanning indicated that the collagen transition was not reversible for all the samples studied. In Fig. 5, the second heating curves are exemplarily shown for the EDC cross-linked scaffold (E) and for the sterilised final product (G).

In addition, some experiments were performed to study the storage stability of some samples in the dry state at room temperature. The storage of non-cross-linked mineralised fibrillar collagen (D) resulted in a change of the collagen properties. It is clear from Fig. 6 that storage under these conditions leads to an intermediate product (H) with higher thermal stability. Probably, covalent bonds increase the size of cooperating units through inter- and intramolecular cross-links and increase the temperature of denaturation (about 20 °C after 2 years storage). Similar processes also occur on natural aging. The nature of the cross-linking might be rather homogeneous, as the width of the peak compared to that of the freshly prepared sample did not increase significantly. By artificial cross-linking of this altered intermediate state with EDC a final product was obtained that differs from (F). In contrast to this, for the cross-linked scaffold (E) there was no significant influence of the storage time in the dry state (up to 4 years) on the thermal behaviour of the swollen scaffolds (Fig. 6 (I)). Thus, the EDC cross-linked scaffolds (E) can be stored for several years, whereas the samples that have not been cross-linked (e.g. D) alter with storage time.

The results presented in this study show that the DSC technique provides a suitable tool for the rapid determination of changes in the protein structure of the different intermediate states during collagen reassembly and mineralisation, scaffold preparation and storage.

3.4. Micro- and nanostructural characterisation

For tissue engineering applications, the macropore diameter of scaffolds seems to be not of great importance, but the interconnected pore diameter should be about 100 μm [42,43]. We have applied several methods to investigate the porosity of the material and its micro- and nanostructural properties. Microcomputed tomography using synchrotron irradiation (SRμ-CT) was carried out with a local resolution of 3.6 μm. A 3D visualisation of the data set is shown in Fig. 7. The method revealed a total porosity of 72%, a surface-to-volume ratio of 0.11 and a mean pore wall thickness of 17.8 μm without many variations in the three directions in space. The mean pore diameter was calculated to be 180 ± 12 μm. These values were confirmed by microscopic evaluations of thin sections, applying methods known

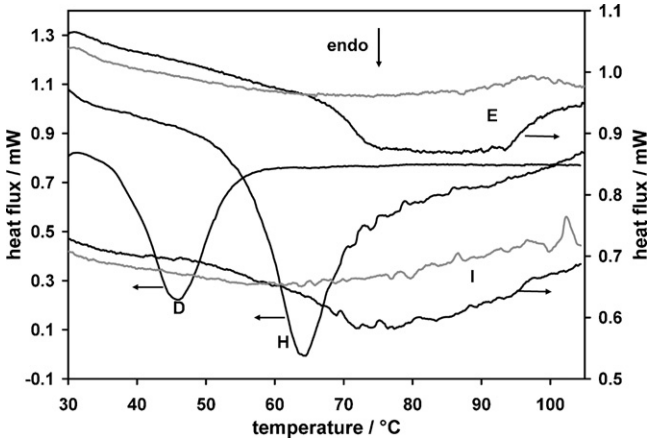

Fig. 6. Storage stability of the non-cross-linked collagen scaffold: DSC plots of a freshly prepared mineralised collagen scaffold swollen in MilliQ water (D) and of a collagen scaffold after two years storage at room temperature (H); and storage stability of the cross-linked collagen scaffold: DSC plots of a freshly prepared collagen scaffold swollen in MilliQ water (E) and of a collagen scaffold after four years storage at room temperature (I); grey plots, second heating; all samples swollen in MilliQ water.

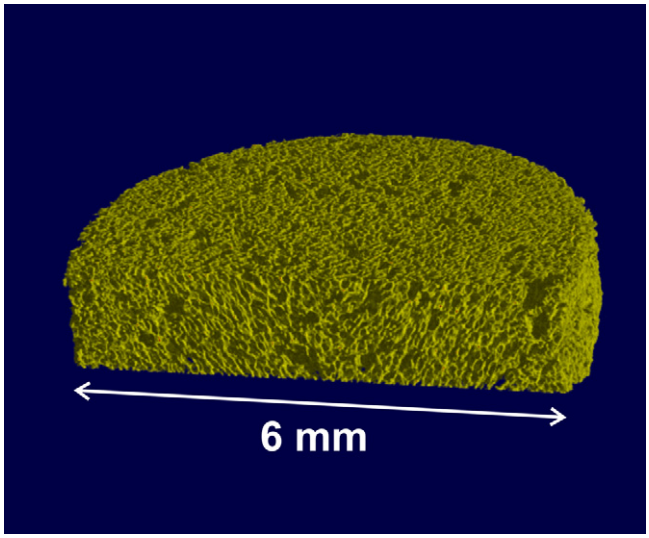

Fig. 7. Result of a microcomputed tomography analysis (SR-μCT) of a porous 3D scaffold of 6 mm diameter (visualisation of the dataset). The porous structure was cut virtually for better clarity.

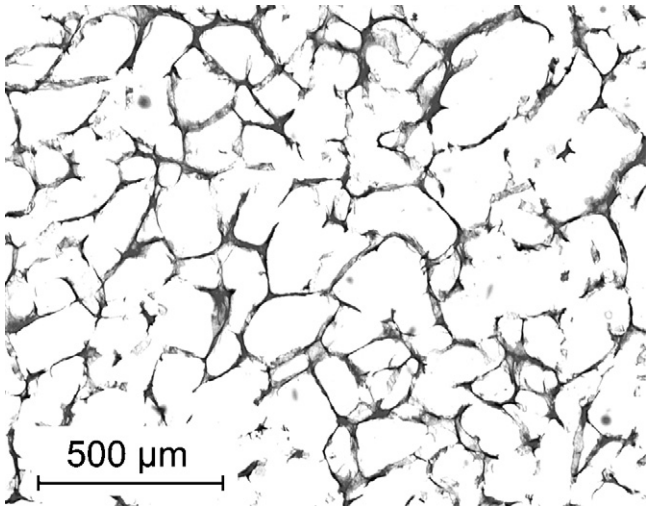

Fig. 8. Light microscopical image of a thin section through a porous mineralised collagen scaffold. For better contrast, the sample was stained with hematoxilin/eosin.

from metallography. In Fig. 8, a light microscopical image of a thin section of the porous mineralised collagen scaffold, stained with hematoxilin/eosin, is presented.

Additionally, the porosity was investigated by intrusion of mercury (Hg porosimetry). A typical graph of the pore size distribution is given in Fig. 9. With this method, pores with diameters of a few nm and up to about 250–300 μm can be detected. In contrast to the microscopical measurement and μ-CT, for Hg porosimetry, the size of pore interconnections counts more than the diameter of the macropores. It is therefore not astonishing that with this method the mean pore size was found to be only 84 ± 3 μm. In the SEM image (Fig. 9) of the scaffold, the diameter of the interconnections pores can be seen. For the total pore area, a value of $48.5 \pm 3\ m^2\ g^{-1}$ was calculated.

The maintenance of the open porous structure and the pore size dimensions under cell culture conditions is a prerequisite for successful cell distribution, adhesion, ingrowth and cultivation. Former experiments demonstrated that the swelling degree

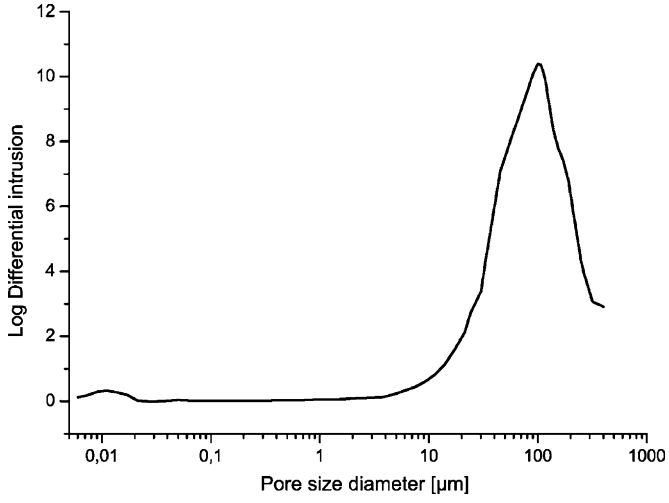

Fig. 9. Typical pore size distribution of a porous 3D scaffold, measured with intrusion of mercury (Hg porosimetry). The mean pore diameter was 84 ± 3 μm.

of the mineralised collagen scaffolds in solvents like distilled water is relatively low in comparison to pure collagen or gelatine matrices [11,44]. The mineralisation of the reconstituted collagen fibrils with nanoscopical HAP crystals therefore stabilises the collagenous network, which is also reflected by the mechanical properties of the mineralised scaffolds (see Section 3.5). For this reason, the pore size in the wet state remained large enough for homogenous cell seeding which is discussed further below (see Section 3.6). As already demonstrated by several other groups, a fast initial freezing of the composite (before lyophilisation) at very deep temperatures leads to much smaller pores which are no longer usable for cell ingrowth [11]. We found −25 °C to be the optimal freezing temperature for the fabrication of porous 3D scaffolds made of mineralised collagen. Higher temperatures (which means slower freezing) resulted in the formation of long, needle-like ice crystals, which are transformed to pores of the same shape during lyophilisation, leading to mechanical instability of the dried scaffold.

The porosity and surface area of porous solids can be conveniently characterised by gas adsorption studies. For the evaluation, nitrogen at 77 K is the most suitable adsorbate. An understanding of the surface area and porosity of an adsorbent can be achieved by the construction of an adsorption isotherm. The quantity of adsorbate on a surface is measured over a wide range of relative pressures at constant temperature. The adsorption isotherm is obtained point-by-point by admitting to the adsorbent successive known volumes of nitrogen and measuring the equilibrium pressure. The Brunauer–Emmett–Teller (BET) method is the most widely used procedure for the determination of the surface area of solid materials and involves the use of the BET equation [45]. The described method supplied information about the pores of the mineralised collagen scaffolds especially in the meso- and microscale (diameters below ca. 400 nm). Table 1 supplies the essential data about the specific surface. In dependence on shape (2D membrane [8] or 3D-scaffold) and collagen source (tendon or skin) a dramatically difference in the value of the specific surface was observed. The flat membrane ("tape"), prepared applying a vacuum filtration process, showed with $88.6\ m^2\ g^{-1}$ the highest specific surface, followed by the porous 3D scaffolds, prepared using collagen I isolated from calf skin ($63.3\ m^2\ g^{-1}$). The standard procedure, described in this paper – formation of porous 3D scaffolds with mineralised collagen from bovine tendon – leads to a material with a specific surface of $30.9\ m^2\ g^{-1}$. Due to the fact that the flat membrane has only pores smaller than 10 μm [8], most of the porosity contributes to the specific surface. In case of the 3D scaffolds most of the pores are in the range of 80–200 μm, resulting in a lower specific surface. The result that with the BET

Table 1
BET specific surface of mineralised collagen samples in variable shapes and made of collagen I from different sources

Material	BET-specific surface ($m^2\ g^{-1}$)
2D-Membrane (collagen I, skin)	88.6
3D-Scaffold (collagen I, skin)	63.3
3D-Scaffold (collagen I, tendon)	30.9

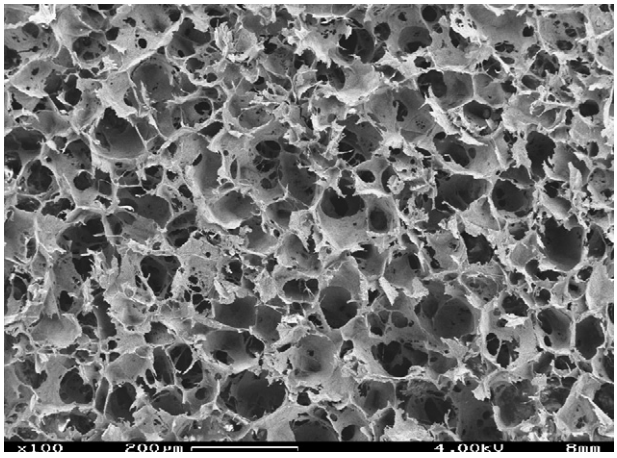

Fig. 10. SEM image of a section through a porous 3D scaffold made of biomimetically mineralised collagen. The interconnectivity of the pores is clearly visible.

method only pores with diameters below 400 nm are recorded may also be the explanation for the differences between the values of specific surface and those of total pore area, achieved with Hg porosimetry. The differences between the two collagen sources may be caused by the different fibril length and diameters; collagen from skin forms during reassembly much smaller and shorter fibrils compared to that from (bovine) tendon. The mineralised composite is therefore much stiffer if tendon collagen is used, and during freezing less micro- and nanopores can be formed.

Scanning electron microscopy confirms the open and interconnecting porosity of the mineralised collagen scaffolds. Fig. 10 (and also Fig. 3A) show sections of a cylindrical sample and the open porosity, necessary for homogeneous cell seeding of the material, is clearly visible. A more detailed description of SEM of the 3D scaffolds has been given in an earlier publication [12].

TEM investigations of thin cuts of the 3D scaffold reveal the mineralisation process of HAP on collagen type I on a mesoscopic scale as well as on atomic level by means of high resolution TEM (HRTEM). Thin cuts of the mineralised and freeze-dried scaffold, embedded in an epoxy resin, were prepared by ultramicrotomy without any staining. The collagen fibrils are therefore not visible due to their low material contrast. As demonstrated in Fig. 11 (left), the collagen framework is partially mineralised by hydroxyapatite. The collagen fibrils – the brightly appearing, elongated structures – are decorated with nanosized HAP crystals aligned along assumed fibril long axis as indicated by zoomed area image (Fig. 11 right). However, at the edges (outer regions) the HAP crystals are less oriented. In Fig. 12 (left), needle or plate-shaped crystals with dimensions between about 15 and 80 nm in length are visible. They are mainly parallel oriented with respect to their long axis. The fibril is bended (bending angle about 110°) and therefore, the crystals on the bottom part of the micrograph show another orientation than those at the top. HRTEM image of Fig. 12 (right) is displaying a HAP needle with a diameter of 3.5 nm. The (1 0 0) lattice planes of about 8.3 Å of hydroxyapatite are revealed which are oriented along the long axis of the crystal. The inset on the right top is displaying the Fast Fourier Transform (FFT) of the crystal; the three most intensive reflexions are indexed. The appearance of our scaffold material in the TEM shows obvious similarity to those of human foetal woven bone [46]. In TEM images of both materials, the calcium phosphate crystals mostly seem to be located on the surface of the collagen fibres instead of being inside the fibrils as in adult, lamellar bone tissue [3].

3.5. Mechanical properties

Due to the fact that biomaterials are exclusively used in the wet state we performed mechanical testing of swollen scaffolds. Porous 3D scaffolds were compressed 50 times uniaxial

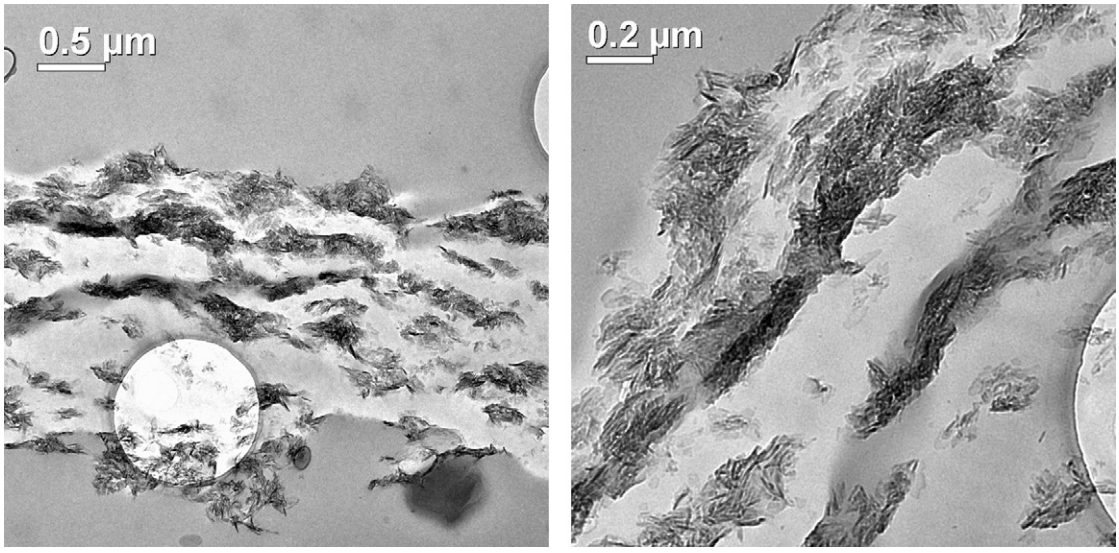

Fig. 11. (Left) Overview TEM image of thin cut of 3D scaffold of hydroxyapatite (HAP) decorated collagen scaffold. (Right) Zoomed area of left hand side micrograph showing mineralised fibrils with nanosized HAP crystals aligned along assumed fibril axis.

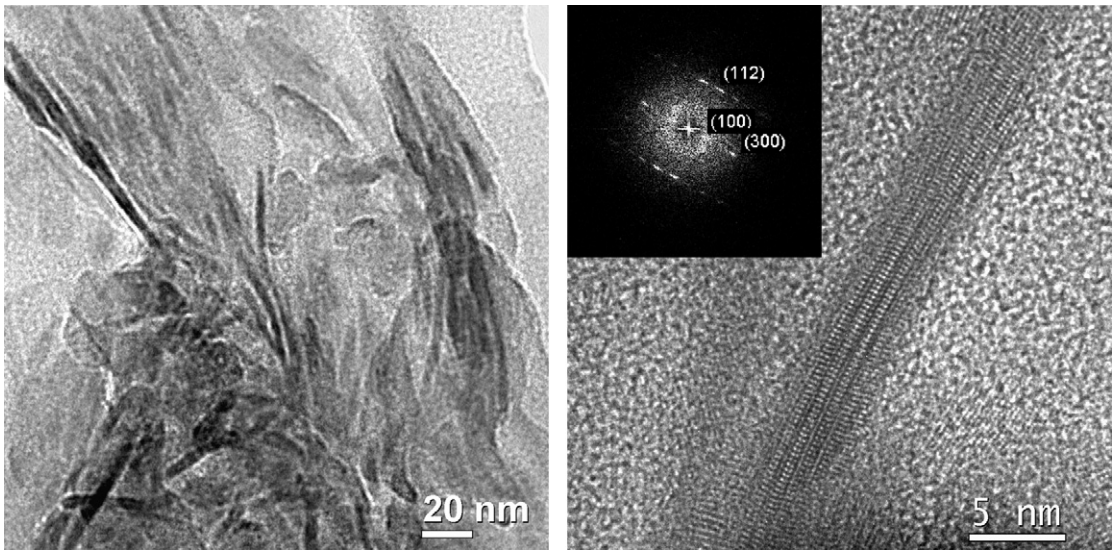

Fig. 12. (Left) Image showing individual needle-like nano Hap crystals with typical length between 15 and 80 nm. They are mainly parallel oriented with respect to each other. (Right) High-resolution TEM micrograph of a HAP needle with a diameter of 3.5 nm diameter. The (1 0 0) lattice planes of about 8.3 Å along the long axis of the needle are clearly visible. The inset on the left top is displaying the Fast Fourier Transform (FFT) of the crystal. Reflections of 8.33 Å (1 0 0), 2.75 Å (3 0 0) and 2.82 Å (1 1 2) of the hexagonal HAP crystal lattice are indicated.

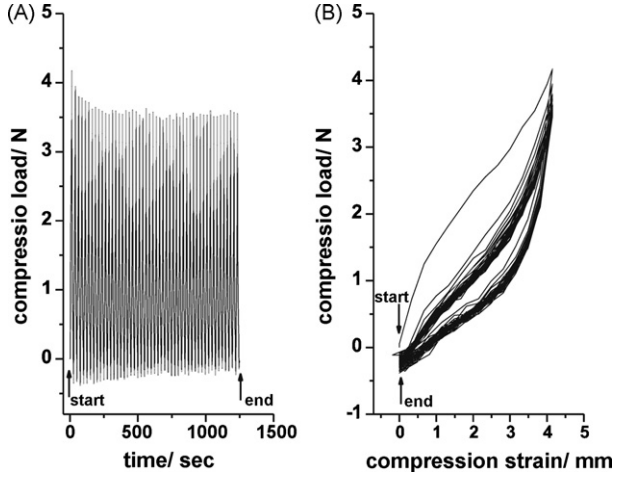

Fig. 13. Cyclic compression test of mineralised 3D scaffold, swollen in distilled water for 24 h. Parameters: uniaxial compression, 50 cycles, chart speed 0.3 mm s^{-1}, 50% compression. (A) Compression load *vs.* time and (B) compression load *vs.* compression strain.

to half of their total height. The compression did not affect the elastic behaviour of the swollen wet scaffolds. For the 50% compression of the cylindrical sample (diameter 13 mm), a compression load of maximal 3.6–3.7 N (resulting in about 28 kPa compressive strength) has been measured. As Fig. 13 illustrates, the scaffold has been slightly deformed after the first 3–4 cycles of the measurement. However, for the following cycles no further inelastic deformation could be detected. The mineralised cross-linked collagen scaffold was able to restore its original shape easily after finishing the tests, which makes cell cultivation under cyclic mechanical stimulation possible. Similar porous scaffolds, made from non-mineralised collagen, show much weaker mechanical properties. We measured under identical conditions a compressive strength of only 2–3 kPa at 50% compression for a porous scaffold, consisting of a non-mineralised collagen I (calf skin)/hyaluronic acid composite, developed for cartilage tissue engineering [47]. Some commercially available (non-mineralised) collagen sponges even collapse spontaneously when wetted. The swelling conditions (in distilled water or 1.5-fold SBF for 24 h both) did not influence the mechanical properties significantly. We have determined in non-cyclic measurements the strength at 20% and 40% compression for both types of swelling conditions; the results are summarised in Table 2.

3.6. Cell seeding and cell response

Cell viability as well as penetration of cells into the inner parts of the scaffold was monitored using MTT staining. MTT is incorporated by viable cells and is intracellularly converted into an insoluble dark blue formazane dye. Therefore, the MTT staining is applicable to visualise the distribution of viable cells macroscopically, which also has been used by other researchers [48,49]. MTT staining indicated the penetration of hMSC from

Table 2
Comparison of the compressive strength for wet mineralised collagen scaffolds after swelling in different media; applied maximum compressive load 50 N (non-cyclic measurement)

Mineralised collagen scaffold	Compressive strength (at 20% compression) (kPa)	Compression strength (at 40% compression) (kPa)
Swollen in distilled water	14.0 ± 0.3	23.5 ± 0.6
Swollen in 1.5× SBF	11.5 ± 0.2	20.7 ± 0.2

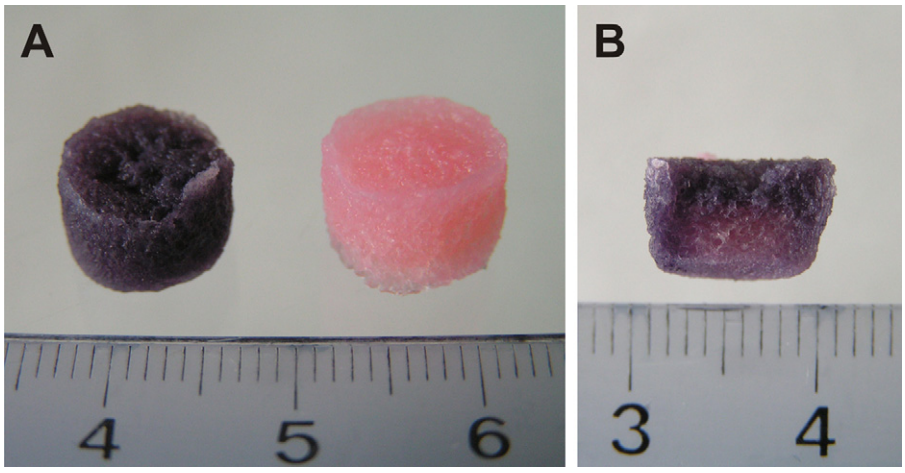

Fig. 14. MTT staining of a mineralised collagen scaffold. (A) Scaffold seeded with 2×10^5 hMSC after 14 days of cultivation (left), compared to control scaffold without cells (right) and (B) longitudinal section of a cell seeded MTT stained scaffold after 14 days of cultivation. The scale bars show centimetres.

the surface throughout the whole depth of the scaffold (Fig. 14A represents a typical image). Analysing sections of formazan stained scaffolds revealed somewhat lower cell densities in the center of the scaffolds (Fig. 14B shows a longitudinal section through a cell seeded and stained scaffold). However, cells attached to the inner parts of the porous scaffolds retained viable over a cultivation time of 14 days. Furthermore, the successful seeding of the inner parts of the mineralised collagen scaffolds was demonstrated by SEM (Fig. 15) [50] as well as cLSM investigations [18]. The effectual penetration of cells into 3D biomaterials seems to be somewhat problematic, even if pore size is sufficient. Niemeyer et al. seeded hMSC to HAP coated collagen I matrices with a pore size from 4 to 200 μm. Already 500 μm below the scaffold surface cells could only be detected in 3 of 10 samples [51]. Limitations with the statical seeding and cultivation of three-dimensional scaffolds were also reported by other groups, who found a restriction of cell ingrowth at 200–250 μm depth [52,53]. We suppose that our seeding method deploying the capillary forces of the scaffolds and the open and interconnecting porosity facilitates the deep penetration of cells.

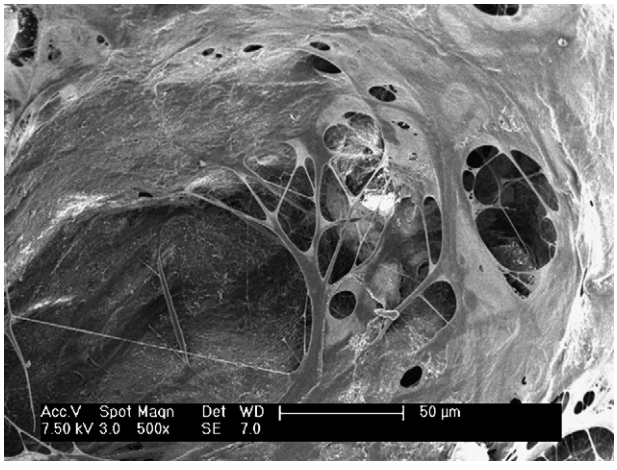

Fig. 15. SEM image of a section through the lower part of cell seeded scaffold, 2 days after seeding.

To maintain cells viable inside such depths the application of perfusion culture seems to be advantageous, but not essential, since we detected a big amount of viable cells inside the scaffolds even after cultivation for several weeks under static conditions.

4. Conclusions

Synchronous mineralisation and fibril reassembly of collagen type I lead to a homogenous nanocomposite material in which the mineral phase HAP is tightly bound to the protein matrix. The close interaction between the nanoscopical HAP crystals and the reconstituted collagen fibrils could be demonstrated with TEM investigations. The porous, three-dimensional scaffolds made of that mineralised collagen type I mimic the composition of extracellular matrix of bone tissue and can therefore be seen as a biomimetic bone graft material. It has been fully characterised concerning its physico-chemical, structural and mechanical properties. The pore size (diameters of about 180 μm) and the open and interconnecting porosity (interconnecting pore diameters of about 80 μm) make deep and homogenous cell seeding possible, which was also proven experimentally. The scaffolds were already tested successfully in several *in vitro* and two *in vivo* experiments. Their elasticity in the wet state enables cell cultivation under cyclic mechanical stimulation. The material and all of its intermediates were characterised by DSC measurements, showing that the mineralisation, fibril reassembly and cross-linking during the preparation process increase the thermal stability of the collagen. γ-Sterilisation of the final product leads to structural changes of the collagen as expected, and part of the molecules becomes damaged. On the other hand, storage of the dry cross-linked and non-sterilised scaffolds over a period of several years did not influence the properties of the protein matrix significantly. This is important to know regarding the application of the developed scaffolds as an implant material in the future.

Due to its closeness to extracellular matrix of healthy bone tissue, the biomimetic porous scaffolds made of mineralised collagen, without or with pre-seeding of cells, can replace autol-

ogous bone graft whose availability is strongly limited and harvesting often connected with donor site morbidity.

Acknowledgements

This work was partly funded by the German Federal Ministry for Education and Research (BMBF) and Biomet Europe (Berlin, Germany). We are grateful to Syntacoll (Saal/Donau, Germany) for generous supply of bovine collagen type I, and want to thank Dr. R. Bernhardt (TU Dresden, TUD), Dr. H. Goebbels and Dr. H. Riesemeier (both Federal Institute of Materials Research/BAM, Berlin, Germany) for the microtomography analysis. We acknowledge Ortrud Zieschang (TUD) and Milauscha Grimmer (Leibniz Institute of Polymer Research Dresden, IPF) for their excellent preparative and analytical work, Professor Wolfgang Pompe for continuous stimulus and Dr. Andreas Sewing for helpful discussions. TEM investigations were carried out at the Triebenberg lab (TUD, Institute of Structural Physics) and thin sections for TEM were prepared by Martina Franke (IPF). BET measurements have been performed by Dr. Victoria Albrecht (IPF, Department Polymer Interfaces) and Hg porosimetry by Dr. Annegret Potthoff (Fraunhofer IKTS, Dresden). Human marrow stromal cells, isolated from bone marrow aspirate, were kindly provided by Sabine Boxberger, Medical Clinic I, and thin section of embedded scaffold was prepared by Ines Kleiber, Maxillofacial Surgery, both Dresden University Hospital.

References

[1] M.K. Sen, T. Miclau, Autologous iliac crest bone graft: should it still be the gold standard for treating nonunions? Injury 38S1 (2007) S75.
[2] D. Wahl, J.T. Czernuszka, Collagen–hydroxyapatite composites for hard tissue repair, Eur. Cells Mater. 11 (2006) 43.
[3] S. Weiner, H.D. Wagner, The material bone: structure–mechanical function relations, Annu. Rev. Mater. Sci. 28 (1998) 271.
[4] J.-Y. Rho, L. Kuhn-Spearing, P. Zioupos, Mechanical properties and the hierarchical structure of bone, Med. Eng. Phys. 20 (1998) 92.
[5] M.A. Rubin, I. Jasiuk, J. Taylor, J. Rubin, T. Ganey, R.P. Apkarian, TEM analyses of the nanostructure of normal and osteoporotic human trabecular bone, Bone 33 (2003) 270.
[6] S.A. Goldstein, R. Goulet, D. McCubbery, Measurement and significance of three-dimensional architecture to the mechanical integrity of trabecular bone, Calcif. Tissue Int. 53 (Suppl. 1) (1993) S127.
[7] J.-H. Bradt, M. Mertig, A. Teresiak, W. Pompe, Biomimetic mineralization of collagen by combined fibril assembly and calcium phosphate formation, Chem. Mater. 11 (1999) 2694.
[8] R. Burth, M. Gelinsky, W. Pompe, Collagen–hydroxyapatite tapes—a new implant material, Tech. Textile 8 (1999) 20.
[9] A. Bernhardt, A. Lode, S. Boxberger, W. Pompe, M. Gelinsky, Mineralised collagen – an artificial, extracellular bone matrix – improves osteogenic differentiation of mesenchymal stem cells, J. Mater. Sci. Mater. Med. 19 (2008) 269.
[10] H. Domaschke, M. Gelinsky, B. Burmeister, R. Fleig, Th. Hanke, A. Reinstorf, W. Pompe, A. Rösen-Wolff, *In vitro* ossification and remodeling of mineralized collagen I scaffolds, Tissue Eng. 12 (2006) 949.
[11] M. Gelinsky, U. König, A. Sewing, W. Pompe, Porous scaffolds made of mineralised collagen—a biomimetic bone graft material, Materialwiss. Werkstofftech. 35 (2004) 229 (in German).
[12] A. Yokoyama, M. Gelinsky, T. Kawasaki, T. Kohgo, U. König, W. Pompe, F. Watari, Biomimetic porous scaffolds with high elasticity made from mineralised collagen—an animal study, J. Biomed. Mater. Res. B: Appl. Biomater. 75B (2005) 464.
[13] M. Scholz, P. Schleicher, C. Koch, F. Friedersdorf, A. Sewing, M. Gelinsky, N.P. Haas, F. Kandziora, Cyclic-RGD is as effective as BMP-2 in anterior interbody fusion of the sheep cervical spine, Eur. Spine J., submitted for publication.
[14] C. Sperling, K. Salchert, U. Streller, C. Werner, Covalently immobilized thrombomodulin inhibits coagulation and complement activation of artificial surfaces *in vitro*, Biomaterials 25 (2004) 5101.
[15] A.R. Boccaccini, J.J. Blaker, Bioactive composite materials for tissue engineering scaffolds, Exp. Rev. Med. Devices 2 (2005) 303.
[16] M. Wang, Developing bioactive composite materials for tissue replacement, Biomaterials 24 (2003) 2133.
[17] M.J. Wissink, M.J. van Luyn, R. Beernink, F. Dijk, A.A. Poot, G.H. Engbers, T. Beugeling, W.G. van Aken, J. Fejen, Endothelial cell seeding on crosslinked collagen: effects of crosslinking on endothelial cell proliferation and functional parameters, Thromb. Haemost. 84 (2000) 325.
[18] A. Bernhardt, A. Lode, C. Mietrach, U. Hempel, Th. Hanke, M. Gelinsky, Biomimetic porous scaffolds from mineralised collagen support growth and osteogenic differentiation of human bone marrow stromal cells, J. Biomed. Mater. Res. A, in press.
[19] J.R. Jones, P.D. Lee, L.L. Hench, Hierarchical porous materials for tissue engineering, Phil. Trans. R. Soc. A 364 (2006) 263.
[20] J. Chakraborty, M.K. Sinha, D. Basu, Biomolecular template-induced biomimetic coating of hydroxyapatite on an SS 316 L substrate, J. Am. Ceram. Soc. 90 (2007) 1258.
[21] A. Reinstorf, M. Ruhnow, M. Gelinsky, U. Hempel, K.-W. Wenzel, P. Simon, W. Pompe, Phosphoserine—a convenient compound for modification of calcium phosphate bone cement collagen composite, J. Mater. Sci. Mater. Med. 15 (2004) 451.
[22] W. Friess, G. Lee, Basic thermoanalytical studies of insoluble collagen matrices, Biomaterials 17 (1996) 2289.
[23] K.J. Payne, A. Veis, Fourier transform IR spectroscopy of collagen and gelatin solutions: deconvolution of the amide I band for conformational studies, Biopolymers 27 (1988) 1749.
[24] F. Flandin, C. Buffevant, D. Herbage, A differential scanning calorimetry analysis of the age-related changes in the thermal stability of rat skin collagen, Biochim. Biophys. Acta 791 (1984) 205.
[25] V.M. Bernal, D.W. Stanley, Stability of bovine muscle connective tissue, J. Food Sci. 52 (1987) 876.
[26] C. Mu, D. Li, W. Lin, Y. Ding, G. Zhang, Temperature induced denaturation of collagen in acidic solution, Biopolymers 86 (2007) 282.
[27] G.C. Na, Monomer and oligomer of type I collagen: molecular properties and fibril assembly, Biochemistry 28 (1989) 7161.
[28] E.I. Tiktopulo, A.V. Kajava, Denaturation of type I collagen fibrils is an endothermic process accompanied by a noticeable change in the partial heat capacity, Biochemistry 37 (1998) 8147.
[29] C.A. Miles, M. Ghelashvili, Polymer-in-a-box mechanism for the thermal stabilization of collagen molecules in fibers, Biophys. J. 76 (1999) 3243.
[30] P.L. Kronick, P. Cooke, Thermal stabilization of collagen fibers by calcification, Connect. Tissue Res. 33 (1996) 275.
[31] H. Trębacz, K. Wójtowicz, Thermal stabilization of collagen molecules in bone tissue, Int. J. Biol. Macromol. 37 (2005) 257.
[32] E. Marzec, L. Kubisz, F. Jaroszyk, Dielectric studies of proton transport in air-dried fully calcified and decalcified bone, Int. J. Biol. Macromol. 18 (1996) 27.
[33] A. Bigi, L. Dovigo, M.H. Koch, M. Morocutti, A. Ripamonti, Collagen structural organization in uncalcified and calcified human anterior longitudinal ligament, Connect. Tissue Res. 25 (1991) 171.
[34] L. Kubisz, S. Mielcarek, F. Jaroszyk, Changes in thermal and electrical properties of bone as a result of 1 MGy-dose irradiation, Int. J. Biol. Macromol. 33 (2003) 89.
[35] P. Angele, R. Kunjat, H. Faltermeier, D. Schuhmann, M. Nerlich, B. Kinner, C. Englert, Z. Ruszczak, R. Mehrl, R. Mueller, Influence of different collagen species on physico-chemical properties of crosslinked collagen matrices, Biomaterials 25 (2004) 2831.
[36] X. Duan, H. Sheardown, Crosslinking of collagen with dendrimers, J. Biomed. Mater. Res. 75A (2005) 510.

[37] C.A. Miles, N.C. Avery, V.V. Rodin, A.J. Bailey, The increase in denaturation temperature following cross-linking of collagen is caused by dehydration of the fibres, J. Mol. Biol. 346 (2005) 551.
[38] A.J. Bailey, Irradiation-induced changes in the denaturation temperature and intermolecular cross-linking of tropocollagen, Radiat. Res. 31 (1967) 206.
[39] C.A. Miles, A. Sionkowska, S.L. Hulin, T.J. Sims, N.C. Avery, A.J. Bailey, Identification of an intermediate state in the helix-coil degradation of collagen by ultraviolet light, J. Biol. Chem. 275 (2000) 33014.
[40] A. Sionkowska, Thermal denaturation of UV-irradiated wet rat tail tendon collagen, Int. J. Biol. Macromol. 35 (2005) 145.
[41] T. Hayashi, S. Curran-Patel, D.J. Prockop, Thermal stability of the triple helix of type I procollagen and collagen. Precautions for minimizing ultraviolet damage to proteins during circular dichroism studies, Biochemistry 18 (1979) 4182.
[42] S. Hofmann, H. Hagenmüller, A.M. Koch, R. Müller, G. Vunjak-Novakovic, D.L. Kaplan, H.P. Merkle, L. Meinel, Control of *in vitro* tissue-engineered bone-like structures using human mesenchymal stem cells and porous silk scaffolds, Biomaterials 28 (2007) 1152.
[43] L. Kong, Q. Ao, A. Wang, K. Gong, X. Wang, G. Lu, Y. Gong, N. Zhao, X. Zhang, Preparation and characterization of a multilayer biomimetic scaffold for bone tissue engineering, J. Biomater. Appl. 22 (2007) 223.
[44] X. Lou, T.V. Chirila, Swelling behaviour and mechanical properties of chemically cross-linked gelatin gels for biomedical use, J. Biomater. Appl. 14 (1999) 184.
[45] L. Safinia, A. Mantalaris, A. Bismarck, Nondestructive technique for the characterization of the pore size distribution of soft porous constructs for tissue engineering, Langmuir 22 (2006) 3235.
[46] X. Su, K. Sun, F.Z. Cui, W.J. Landis, Organization of apatite crystals in human woven bone, Bone 32 (2003) 150.
[47] M. Gelinsky, M. Eckert, F. Despang, Biphasic, but monolithic scaffolds for the therapy of osteochondral defects, Int. J. Mater. Res. 98 (2007) 749.
[48] S.S. Kim, C.A. Sundback, S. Kaihara, M.S. Benvenuto, B.-S. Kim, D.J. Mooney, J.P. Vacanti, Dynamic seeding and *in vitro* culture of hepatocytes in a flow perfusion system, Tissue Eng. 6 (2000) 39.
[49] J.R. Mauney, J. Blumberg, M. Pirun, V. Volloch, G. Vunjak-Novakovic, D.L. Kaplan, Osteogenic differentiation of human bone marrow stromal cells on partially demineralized bone scaffolds *in vitro*, Tissue Eng. 10 (2004) 81.
[50] A. Lode, A. Bernhardt, S. Boxberger, M. Gelinsky, Cultivation of mesenchymal stem cells on a three-dimensional artificial extracellular bone matrix, in: A.J. Nadolny (Ed.), Proceedings of the International Conference "Biomaterials in Regenerative Medicine", Conference Proceedings and Monographs, vol. 6, Vienna Scientific Centre of the Polish Academy of Sciences, 2006, pp. 167–172.
[51] P. Niemeyer, U. Krause, J. Fellenberg, P. Kasten, A. Seckinger, A.D. Ho, H.G. Simank, Evaluation of mineralized collagen and alpha-tricalcium phosphate as scaffolds for tissue engineering of bone using human mesenchymal stem cells, Cells Tissues Organs 177 (2004) 68.
[52] S.L. Ishaug-Riley, G.M. Crane-Krüger, M.J. Yaszemski, A.G. Mikos, Three-dimensional culture of rat calvarial osteoblasts in porous biodegradable polymers, Biomaterials 19 (1998) 1405.
[53] T. Mygind, M. Stiehler, A. Badrup, H. Li, X. Zhou, A. Flyvbjerg, M. Kassem, C. Bünger, Mesenchymal stem cell ingrowth and differentiation on coralline hydroxyapatite scaffolds, Biomaterials 28 (2007) 1036.